Increased Quasi Stationarity and Persistence of Winter Ural Blocking and Eurasian Extreme Cold Events in Response to Arctic Warming. Part II: A Theoretical Explanation

DEHAI LUO AND YAO YAO

Key Laboratory of Regional Climate-Environment for Temperate East Asia, Institute of Atmospheric Physics, Chinese Academy of Sciences, Beijing, China

AIGUO DAI

Department of Atmospheric and Environmental Sciences, University at Albany, State University of New York, Albany, New York, and National Center for Atmospheric Research, Boulder, Colorado

IAN SIMMONDS

School of Earth Sciences, University of Melbourne, Parkville, Victoria, Australia

LINHAO ZHONG

Key Laboratory of Regional Climate-Environment for Temperate East Asia, Institute of Atmospheric Physics, Chinese Academy of Sciences, Beijing, China

(Manuscript received 30 March 2016, in final form 30 December 2016)

ABSTRACT

In Part I of this study, it was shown that the Eurasian cold anomalies related to Arctic warming depend strongly on the quasi stationarity and persistence of the Ural blocking (UB). The analysis here revealed that under weak mean westerly wind (MWW) and vertical shear (VS) (quasi barotropic) conditions with weak synoptic-scale eddies and a large planetary wave anomaly, the growth of UB is slow and its amplitude is small. For this case, a quasi-stationary and persistent UB is seen. However, under strong MWW and VS (quasi baroclinic) conditions, synoptic-scale eddies are stronger and the growth of UB is rapid; the resulting UB is less persistent and has large amplitude. In this case, a marked retrogression of the UB is observed.

The dynamical mechanism behind the dependence of the movement and persistence of UB upon the background conditions is further examined using a nonlinear multiscale model. The results show that when the blocking has large amplitude under quasi-baroclinic conditions, the blocking-induced westward displacement greatly exceeds the strong mean zonal-wind-induced eastward movement and hence generates a marked retrogression of the blocking. By contrast, under quasi-barotropic conditions because the UB amplitude is relatively small the blocking-induced westward movement is less distinct, giving rise to a quasi-stationary and persistent blocking. It is further shown that the strong mid–high-latitude North Atlantic mean zonal wind is the quasi-barotropic condition that suppresses UB's retrogression and thus is conducive to the quasi stationarity and persistence of the UB. The model results show that the blocking duration is longer when the mean zonal wind in the blocking region or eddy strength is weaker.

1. Introduction

Atmospheric blocking is known to have significant impacts on parts of Eurasia (Luo et al. 2016a,b). In Yao et al. (2017, hereafter Part I), we examined the association of cold and warm anomalies over Eurasia with changes in the background flow conditions, namely, the strength of the mean westerly wind (MWW) and its vertical shear (VS) associated with Arctic warming and Arctic sea ice decline over the Barents and Kara Seas (BKS). It was found that the quasi stationarity and persistence of Ural blocking (UB) are instrumental in determining the persistence, robustness, and location of cold anomalies over Eurasia. Small-amplitude UB

Corresponding author e-mail: Dr. Dehai Luo, ldh@mail.iap.ac.cn

DOI: 10.1175/JCLI-D-16-0262.1

events, as seen in a quasi-barotropic environment, are important for the presence of strong and persistent cold anomalies over central and East Asia because of their quasi stationarity and persistence over the Ural region. By contrast, the occurrence of large-amplitude UB events in a quasi-baroclinic environment has little influence on cold anomalies over central and East Asia because the block moves rapidly westward. However, the block can then produce cold anomalies over Europe. But what determines the quasi stationarity and persistence of UB patterns remains unclear, and this is addressed here with a nonlinear theoretical model.

As noted by Walsh (2014), the role of the Arctic warming associated with sea ice loss (Simmonds 2015) is likely to weaken the midlatitude mean westerly wind to favor a meandering westerly jet stream (blocking). Francis and Vavrus (2015) also suggested that the Arctic warming can favor large-amplitude wavy flows to generate extreme cold events, although the physical cause of the regionality and magnitude of extreme cold events is still subject to debate (e.g., Screen and Simmonds 2013a,b; Screen et al. 2014; Overland et al. 2015). This issue can be investigated using data analysis (as in Part I) and a theoretical model that can capture the blocking life cycle in specific regions.

Over the past few decades, a number of theoretical models have been proposed to explain the maintenance of blocking flows (Charney and DeVore 1979; McWilliams 1980; Shutts 1983). However, these models failed to describe the life cycle of blocking, and thus it is not possible to use them to examine how the duration, position (movement), and intensity of blocking depend on the background conditions. Luo (2000, 2005), Luo and Li (2000), and Luo et al. (2001, 2014) have recently proposed and developed a nonlinear multiscale interaction (NMI) model to describe the life cycle of a blocking (a meandering westerly jet stream) based on the notion that the blocking flow is essentially a nonlinear initial value problem. This viewpoint is consistent with the results obtained from the conditional nonlinear optimal perturbation (CNOP) method (Mu and Jiang 2008). In the NMI model, the blocking flow is generated by the forcing of preexisting synoptic-scale eddies, and their interaction with the planetary waves and mean flow existed prior to the block onset (Luo 2000; Luo and Li 2000; Luo et al. 2001). This model can capture the life cycle of the observed blocking event (Berggren et al. 1949) and its main features (Luo 2000, 2005; Luo et al. 2001, 2014). It also reveals how the period length, intensity, and movement of a blocking event depend on three key parameters, namely, the strength and structure of the preexisting planetary wave (an incipient block), preexisting synoptic-scale eddies, and mean zonal wind (Luo 2000). As noted in Part I and below, the variations of these parameters are closely related to the Arctic warming over the BKS. Thus, the NMI model used in this paper can allow us to provide an explanation for why a UB pattern becomes more quasi stationary and persistent under a quasi-barotropic condition (with weak MWW, VS, and synoptic-scale eddies) associated with Arctic warming over the BKS.

This paper is organized as follows: In section 2 the data and methodology are described. The results related to the link between a UB and the background conditions are presented in section 3. In section 4, some theoretical results from the NMI model are presented to account for the physical cause of quasi-stationary and persistent UB patterns under weak MWW or VS conditions. We reveal how the duration of the UB dipole depends on the background condition changes in section 5, and the main conclusions and discussion are given in section 6.

2. Data, methods, and the NMI model

The data used here are the daily 500-hPa geopotential height, multilevel wind, and surface air temperature (SAT) available from the National Centers for Environmental Prediction (NCEP)–National Center for Atmospheric Research (NCAR) reanalysis dataset (Kalnay et al. 1996) for the winter [December–February (DJF)] during the period from December 1950 to February 2015 (1951–2015) with a 2.5° × 2.5° resolution (http://www.esrl.noaa.gov/psd/data/gridded/data.ncep.reanalysis. html). The selected UB events we use here are the same as in Part I. As in Part I, we calculated the composite DJF-mean wind fields to obtain the background condition by removing daily wind fields associated with the blocking life cycle. In the present work, the NMI model developed by Luo (2000, 2005), Luo and Li (2000), and Luo et al. (2001, 2007, 2014), as described in appendix A, is used to reveal the physical cause of the impact of the background conditions on the lifetime and movement of UB patterns.

3. Link between the movement and persistence of UB events and the background condition changes

Although the fact that the length of the UB duration is related to the MWW and VS strengths has been mentioned in Part I, we did not quantify the link between the movement and persistence of the UB pattern and the background conditions in the blocking region and its upstream side. In fact, as noted below, the movement and persistence of the UB pattern are related not only to the background conditions in the blocking region but also to upstream conditions. In this section, we will examine the two issues to compare their different roles. Before

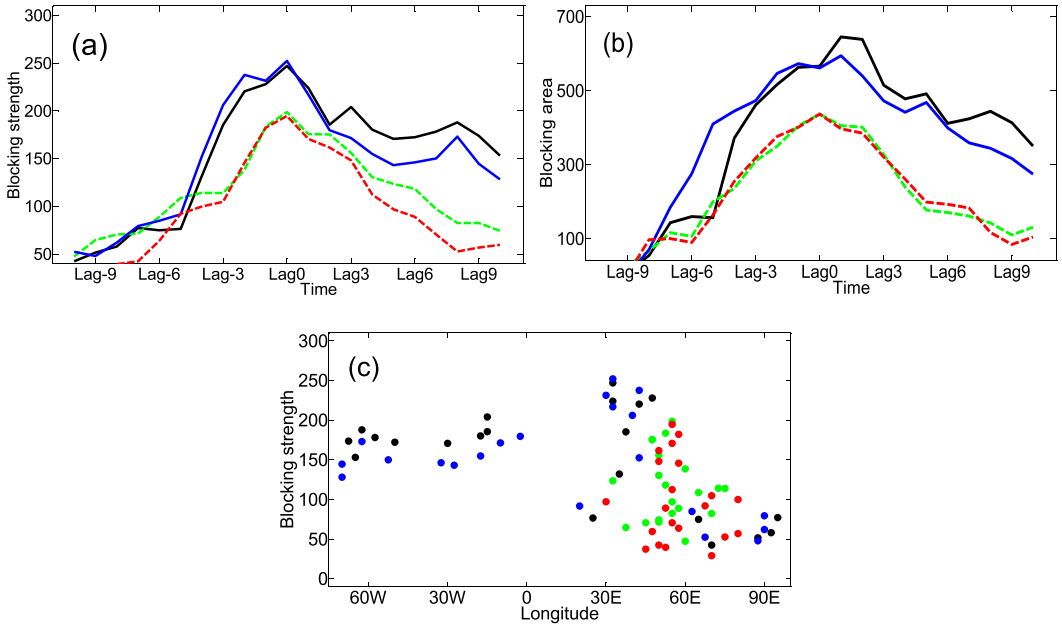

FIG. 1. (a) Time evolution of the maximum amplitude of the anticyclonic center (blocking strength; gpm) of composite daily 500-hPa geopotential height anomalies of UB events and (b) the blocking area ($\times 10^6$ km^2) for 500-hPa height anomalies ≥60 gpm for strong MWW (black)–VS (blue) and weak MWW (green)–VS (red) winters; (c) the blocking intensity (gpm) against the zonal position (longitude) of the maximum anticyclonic center of the composite daily height anomaly. Lag 0 day denotes the blocking peak.

examining these problems we first define the UB to be quasi stationary if the anticyclonic center of the UB pattern lies in the longitude range from 30° to 90°E (the Ural region, as defined in Part I) during its life cycle. Otherwise, it is defined to be a mobile blocking event. Correspondingly, the number of days for which the center is found in the Ural region is defined to be its persistence time.

a. The background conditions in the blocking region

As a further quantification of the UB behavior we define the maximum amplitude of the anticyclonic center of the blocking dipole as the blocking strength, and the weighted mean area over which the positive height anomalies exceed 60 gpm is defined as the magnitude of the blocking area. We also define the longitude where the anticyclonic center of the blocking dipole is located as the blocking location.

To compare with the theoretical result (see Fig. 10), it is necessary to show the time variations of the composite daily blocking strength and blocking area as well as the zonal location (longitude) of blocking events in Fig. 1 during its blocking life cycle for weak and strong MWW or VS winters. It is seen that the blocking strength (area) is stronger (wider) for the strong MWW or VS (black and blue lines in Figs. 1a,b) than for the weak MWW or VS (green and red lines in Figs. 1a,b), whereas the location of the anticyclonic center is distributed in a more widespread zonal region for the strong MWW or VS (black and blue dots in Fig. 1c) than it is for the weak MWW or VS. This reflects that the blocking dipole shows a marked zonal shift from Eurasia to the North Atlantic during its life cycle for the strong MWW or VS. However, for the weak MWW or VS the anticyclonic center of the blocking dipole is mainly confined to the Ural region (around 60°E). On the other hand, we can see from the time evolution of the maximum blocking amplitude that the blocking dipole appears to have a long duration for the strong MWW or VS (black and blue lines in Fig. 1a). However, this does not mean that the blocking dipole is more persistent over the Ural region (solid line in Fig. 9a of Part I). In contrast, it is short lived because it retrogrades rapidly away from the Ural region. Although the mean zonal wind is weaker, the blocking dipole is seen to be more quasi stationary and persistent over the Ural region for the weak MWW or VS (dashed line in Fig. 8b of Part I). This implies that other factors, such as the upstream conditions noted below, may play an important role in determining the quasi stationarity and persistence of the UB pattern. As in Part I, we may still refer to the strong (weak) MWW and VS over the Ural region as a quasi-baroclinic (quasi barotropic) condition.

It is further apparent from Fig. 1a that the growth of the UB is more (less) rapid and prominent under a quasi-baroclinic (quasi barotropic) condition. This reflects the fact that the UB can easily reach large amplitude only

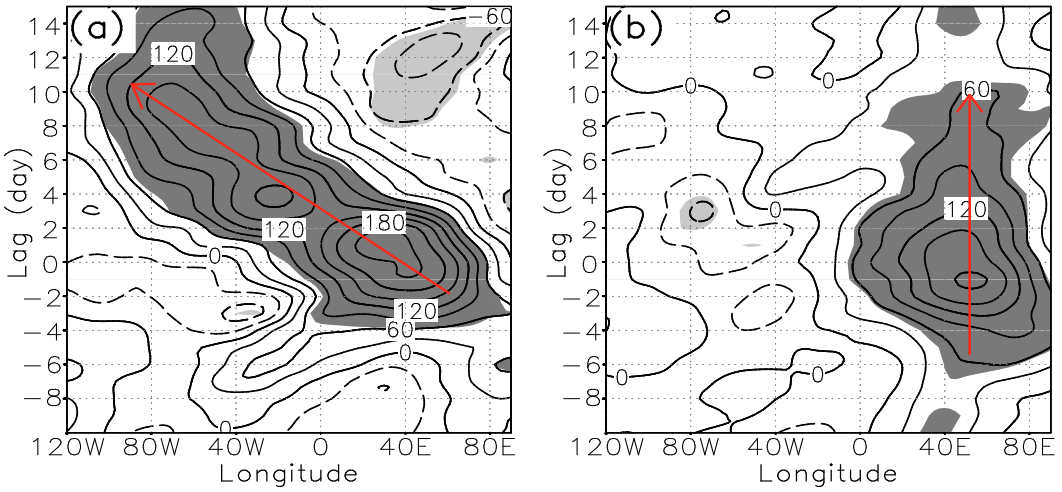

FIG. 2. Time–longitude evolution of composite daily 500-hPa geopotential height anomalies averaged over 60°–70°N of UB events for (a) strong and (b) weak MWW winters during 1951–2015. The shading denotes the region above the 95% confidence level. The red arrow denotes the movement direction of the UB anticyclone.

under quasi-baroclinic conditions (Luo 2000). In other words, the weak MWW or VS tends to favor the slow growth of the UB and its small amplitude. As a result, we see that the slow zonal movement of the UB is related not only to the small amplitude of the UB but also likely to upstream background conditions, as noted below. These two points represent new findings over and above those presented in Part I.

To explain the difference of the zonal location of blocking between the quasi-baroclinic and quasi-barotropic conditions, it is useful to plot the time–longitude evolution of the composite daily 500-hPa geopotential height anomaly averaged over the region 60°–70°N during the blocking life cycle to quantify their different zonal movements under different background conditions. The results are shown in Fig. 2 for the strong and weak MWW cases. It is noted that the anticyclonic anomaly shows a distinct westward displacement for the strong MWW (Fig. 2a) but is almost immobile and remains in a narrow zonal region near 60°E for the weak MWW (Fig. 2b). Because the UB has large amplitude for the strong MWW and VS, one is led to conclude that the marked retrogression of the blocking dipole over Eurasia for the strong MWW is closely related to its large amplitude, even though the mean flow over mid–high-latitude Eurasia is relatively strong. In contrast, for the weak MWW the quasi stationarity of the UB is likely due to its small amplitude. These results also hold for the strong and weak VS cases (not shown). Such a zonal movement of the UB pattern cannot be explained by linear Rossby wave theory, but, as we shall see shortly, it may be explicated using our nonlinear theory (see appendix A). This encourages us to investigate the upstream conditions and winter planetary wave anomalies before a nonlinear theoretical model is used, as the model makes use of the mean flow, the strengths of synoptic-scale eddies upstream, and the planetary wave prior to the block onset.

b. *Upstream conditions and winter planetary wave anomalies associated with the UB changes*

Guided by the above considerations we now explore what spatial patterns of the mean zonal wind, vertical shear, and synoptic-scale eddies correspond to the increased quasi stationarity and persistence of UB. In addition to the DJF-mean westerly wind $U_{300}(x, y)$ and its vertical shear $U_T(x, y)$ as defined in Part I, here we define the DJF-mean 300-hPa eddy kinetic energy (EKE) (the synoptic-scale eddies are defined as the high-passed transients for a 2.5–7-day Butterworth filter) for UB events being excluded as the EKE strength $E_{\text{eke}}(x, y)$. To investigate the connection among $U_{300}(x, y)$, $U_T(x, y)$, and $E_{\text{eke}}(x, y)$, along with the increased quasi stationarity and persistence of the UB, it is helpful to perform the regressions of the anomalies of these three atmospheric parameters against the time series of the normalized UB frequency (solid line in Fig. 3c of Part I). Figures 3a–c show that, while the increased UB frequency corresponds to a large reduction of $U_{300}(x, y)$, $U_T(x, y)$, and $E_{\text{eke}}(x, y)$ over mid–high-latitude Eurasia, an increase in $U_{300}(x, y)$ and $U_T(x, y)$ in the North Atlantic high-latitude region near Greenland is not particularly evident. The decrease in the DJF-mean EKE is rather distinct over Europe and the North Atlantic as the UB days increase and is intensified over the BKS (Fig. 3c). On the other hand, as we have noted in Part I, the intensification of the mean zonal wind and its vertical shear over the North

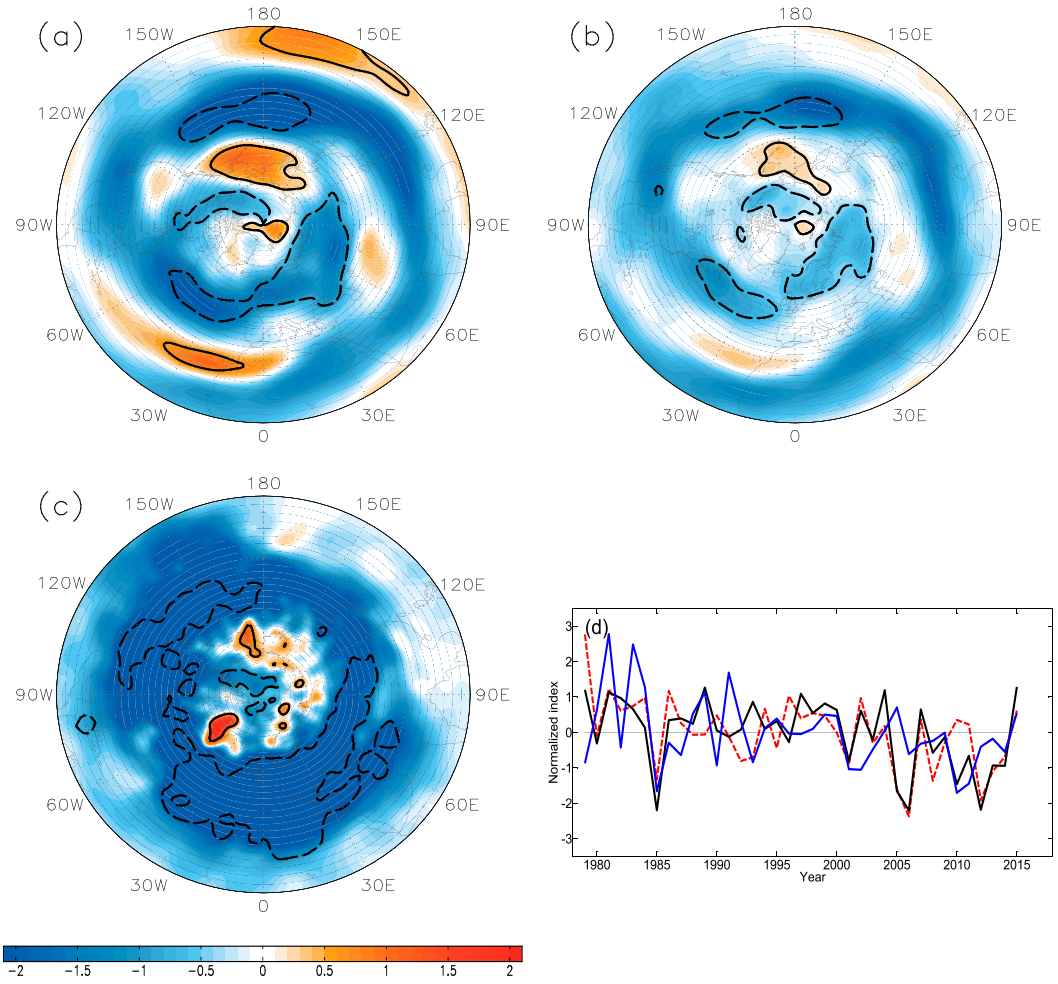

FIG. 3. The regression maps of the DJF-mean (a) 300-hPa zonal wind (m s^{-1}), (b) vertical shear (s^{-1}), and (c) 300-hPa EKE (m^2 s^{-2}) anomalies regressed against the normalized UB frequency time series (solid line in Fig. 3c of Part I), as well as (d) time variations of normalized U_{300A} (black), VS_A (red), and E_{Meke} (blue). In (a)–(c), the dashed curve represents the area above the 95% confidence level for a two-sided Student's t test.

Atlantic mid-to-high latitudes is prominent as the Arctic warming takes place over the BKS, while their significant weakening is seen over mid–high-latitude Eurasia (Figs. 2e,f of Part I). Moreover, below we can further see that the mean zonal wind and its vertical shear over mid–high-latitude Eurasia show strength variations opposite to those over North Atlantic mid-to-high latitudes. In other words, the mid–high-latitude westerly wind is strong over the North Atlantic but weak over Eurasia for a weak MWW or VS winter. Such a zonal distribution of the mean zonal wind can explain why the UB is slowly (rapidly) westward moving in the zonal direction under quasi-barotropic (quasi baroclinic) conditions.

Many studies have indicated that upstream eddy vorticity forcing plays a key role in the establishment of the blocking dipole (Berggren et al. 1949; Shutts 1983; Holopainen and Fortelius 1987) because the large-scale topography plays a secondary role in generating blocking flows compared to that of preexisting synoptic-scale eddies (Luo 2005). Thus, in this paper we only consider preexisting synoptic-scale eddies to emphasize their role in the blocking life cycle.

We define the value of $E_{eke}(x, y)$ averaged over the region 40°–70°N, 10°W–30°E as the strength E_{Meke} of preexisting synoptic-scale eddies (preexisting or background eddy strength as defined below). The choice of this upstream averaging domain is based on observational (Colucci 1985; Holopainen and Fortelius 1987; Murray and Simmonds 1995; Inoue et al. 2012) and theoretical (Luo 2000) analysis, which indicates that the upstream synoptic-scale eddies prior to the block onset can drive downstream blocking. Luo et al. (2016b) found that the eddy vorticity forcing is mainly located in the European continent upstream of the Ural region.

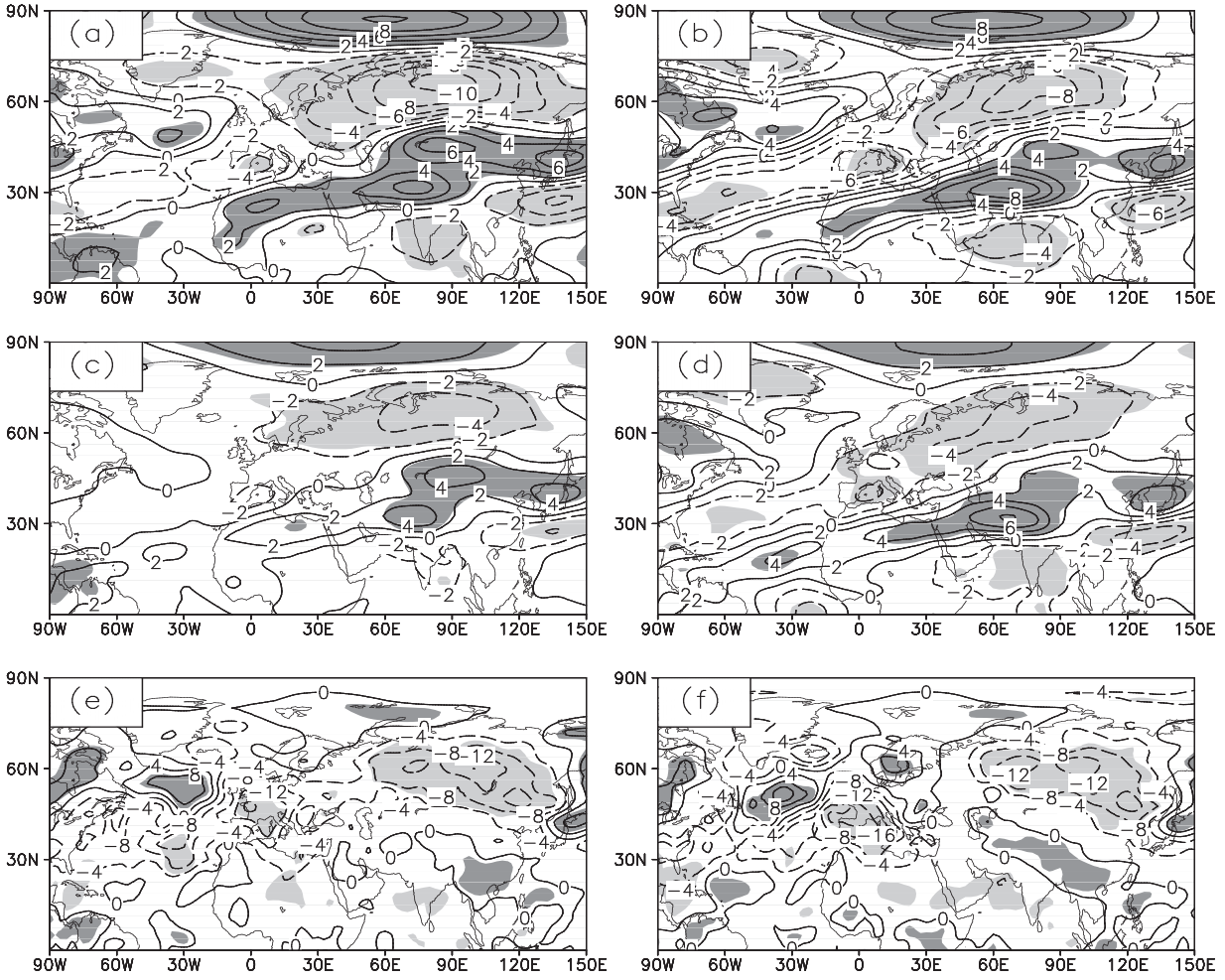

FIG. 4. The difference of the horizontal distribution of the composite: (a),(b) MBW $U_B(x, y)$; (c),(d) vertical shear U_T; and (e),(f) 300-hPa EKE between: (a),(c),(e) weak and strong MWW and (b),(d),(f) weak and strong VS winters. The shading denotes the region above the 95% confidence level.

Hence, E_{Meke} over Europe may be used as an index of a meteorological parameter that affects UB variability, in addition to the 300-hPa mean zonal wind $U_{300\text{A}}$ and its vertical wind shear VS_A (as described in Part I) within the blocking region as the background parameters.

We show the time series of the normalized $U_{300\text{A}}$, VS_A, and E_{Meke} in Fig. 3d. Correlation analysis shows that while $U_{300\text{A}}$ and VS_A have a positive correlation of 0.72 (0.66) for a nondetrended (detrended) case, E_{Meke} has a downward trend and does not exhibit a significant correlation with $U_{300\text{A}}$ and VS_A, whose correlation coefficients are 0.39 and 0.18 (0.30 and 0.02), respectively. The magnitudes of these correlations reflect the fact that the upstream EKE does not depend on the downstream background conditions, whereas it does depend on the upstream conditions over Europe and North Atlantic.

It is meaningful to examine the spatial distribution of the mean zonal wind to understand what affects the zonal movement of the UB. Here, we define the vertical average of DJF-mean zonal winds for UB events being excluded between the 700- and 200-hPa levels as the mean barotropic zonal wind (MBW) $U_B(x, y)$ in winter. We show the difference of the horizontal distribution of the composite $U_B(x, y)$ field between weak and strong MWW (VS) winters in Fig. 4a (Fig. 4b). One can see that the MBW is stronger over the North Atlantic but weaker over Eurasia (mainly over the Ural region) for the weak MWW (Fig. 4a) or VS (Fig. 4b) winters compared to the strong MWW or VS winters. To some extent, the strong (weak) mean westerly wind over the North Atlantic mid-to-high latitudes suppresses (encourages) the retrogression of blocking dipole over Eurasia for a weak (strong) MWW or VS. Such a mean zonal wind distribution in the North Atlantic is the upstream condition of the UB movement. This is probably the reason why the UB is quasi stationary (rapidly westward traveling) under a quasi-barotropic

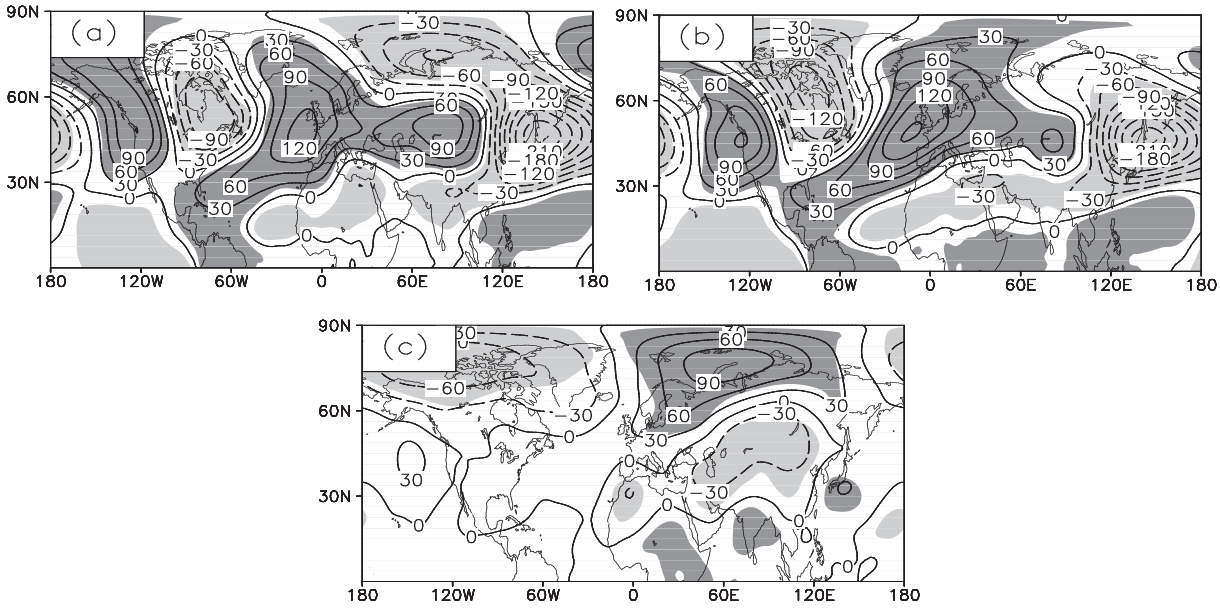

FIG. 5. The DJF-mean 500-hPa geopotential height anomaly deviation from a zonal mean for (a) strong MWW winters, (b) weak MWW winters during 1951–2015, and (c) their differences [(b) − (a)], in which the solid (dashed) lines represent positive (negative) values. The shading denotes the area above the 95% confidence level.

(quasi baroclinic) condition, while the large amplitude of the blocking dipole is also important for its retrogression, as noted below. As further revealed in Part I (their Fig. 2f), the strong (weak) westerly wind in high latitudes of the North Atlantic (Eurasia) is closely related to the warming over the BKS. Thus, quasi-stationary and persistent UB is a result of the BKS warming.

Correspondingly, the difference of the composite $U_T(x, y)$ field between weak and strong MWW (VS) winters is shown in Fig. 4c (Fig. 4d). We can see from Fig. 4c that the difference of the composite $U_T(x, y)$ between weak and strong MWW winters has negative values over 0°–120°E, 50°–80°N but is weakly positive over the North Atlantic, thus implying that the background baroclinicity is weaker over Eurasia but slightly stronger over the North Atlantic in weak compared with strong MWW winters. This result can also be seen from the difference of the composite $U_T(x, y)$ field between weak and strong VS winters (Fig. 4d), although there is a small difference between Figs. 4c,d. Thus, the increased (decreased) vertical wind shear over the North Atlantic (Eurasia) seems to be related to the Arctic warming over the BKS, as noted in Part I (their Fig. 2e). A larger reduction of the DJF-mean EKE is also seen over Europe for weak compared with strong MWW winters (Fig. 4e), while such a reduction is also large over Europe from strong to weak VS winters (Fig. 4f).

Although the background condition change is associated with the intensified Arctic warming as revealed in Part I, it is also useful to estimate changes in the regionally averaged MBW and VS over the region 50°–75°N, 30°–90°E and E_{Meke} from the strong to weak MWW winters. The calculation shows that the values of the MBW were 12.5 and 7.9 m s^{-1} for strong and weak MWW winters, respectively, representing a difference of 36.8%. A similar calculation for the VS gives 7.6 and 5 s^{-1}, a 34.2% difference, while the corresponding values for E_{Meke} are 51 and 45.5 m^2 s^{-2}, a reduction of 11% for the weak MWW winter cases. Thus, in our model calculation the small (large) values of the background westerly wind u_0 and eddy strength a_0, as defined in appendix A, should be chosen for the weak (strong) MWW or VS winters, although the variation of E_{Meke} is mainly affected by the North Atlantic condition rather than by the strength of VS over the Ural region.

We show the DJF-mean 500-hPa geopotential height anomalies for UB events being excluded in Fig. 5 for strong and weak MWW winters. It is seen that the winter-mean planetary wave anomaly is stronger for weak (Fig. 5b) than for strong MWW (Fig. 5a) winters. This can be most clearly seen from the difference of the DJF-mean height anomaly between the weak and strong MWW winters (Fig. 5c). The difference field shows that a positive-over-negative dipole anomaly appears over a region stretching from the BKS to the south side of Ural Mountains and from 30° to 90°E. This result can also be found for weak VS winters (not shown). Because of the presence of this dipole anomaly the UB days are increased for the weak MWW or VS winters. In other words, the presence of a positive-over-negative dipole anomaly over the Ural region

tends to increase the persistence of UB events for the weak MWW or VS winters.

4. Theoretical results and their dynamical explanation

As noted above, the NMI model is able to realistically describe the life cycles of observed blocking events and their main characteristics (Luo 2000, 2005; Luo and Li 2000; Luo et al. 2001, 2014). This gives us great confidence that the model can be used to quantify the relationships between the life cycle (intensity, position, or movement and duration) of the UB dipole and changes in the background conditions, even though this barotropic model might not be thought applicable for investigations of the consequences of quasi-baroclinic environment. However, we can justify such an application as discussed below.

As explained in appendix A, in this model, the three key inputs to the model are the strength of background westerly wind within the blocking region denoted by u_0, the strength of preexisting synoptic-scale eddies prior to the block onset in the upstream region of the blocking flow denoted by a_0 (or preexisting eddy strength as above), and the initial amplitude of the dipole planetary wave $B(x, 0)$. This NMI model is idealized in the sense that the vertical mean wind shear has been neglected [the two-layer baroclinic form of an NMI model is presented in Luo (2000)]. However, the model can still be used to investigate the zonal movement of the UB dipole in a quasi-baroclinic environment if the blocking amplitude can be assumed to be the same as in the quasi-baroclinic condition, even though the observed UB anomaly exhibits an asymmetric dipole. We make the assumption in the model that the barotropic mean zonal wind is uniform in the zonal and meridional directions. For our purpose, the parameters u_0, $B(x, 0)$, and a_0 of the NMI model used in this study are not fixed, while the other parameters are fixed and chosen to be the same values as in Luo et al. (2014).

a. *The impact of the mean westerly wind strength*

To ascertain the impact of the background westerly strength on the duration, intensity, and movement of the blocking dipole, here we fix $B(x, 0) = 0.4$ and $a_0 = 0.17$, while varying the value of u_0. We show the instantaneous planetary-scale and total fields of a blocking dipole obtained from the NMI model in Fig. 6 for $u_0 = 0.9$ ($9\,\mathrm{m\,s^{-1}}$ in dimensional form) (Fig. 7, $u_0 = 0.6$; $6\,\mathrm{m\,s^{-1}}$). It is seen that when the mean westerly wind u_0 is stronger, the eddy-driven blocking dipole is relatively weak and less persistent (Fig. 6a for $u_0 = 0.9$), which undergoes a slow eastward movement. This result is held only for the case without the effect of VS. The blocking dipole becomes strong once the strong vertical wind shear is included (Luo 2000). The eddy-driven blocking dipole is strong and long lived and travels rapidly westward when the mean westerly wind u_0 is weak (Fig. 7a for $u_0 = 0.6$). In particular, Figs. 6b and 7b show that when the background westerly wind is weaker, the total field of the blocking flow exhibits a strong westerly jet meandering. For this case, the intense cold air shifts southward to induce a cooling in midlatitude regions. Thus, it is likely that the Arctic warming leads to a large meandering of the westerly jet streams to generate extreme cold events over Eurasia because of the appearance of a blocking flow through the weakening of the mid–high-latitude westerly winds over Eurasia. This case is likely over Eurasia because of the Arctic warming due to the sea ice loss over the BKS. Thus, the weak uniform background westerly wind over Eurasia can increase the lifetime of blocking dipole and favor its retrogression. Its retrogression is suppressed so that it becomes quasi stationary once a strong mean zonal wind over the North Atlantic is included in this model, as noted below.

b. *Impact of the preexisting synoptic-scale eddy strength*

Because an increased UB frequency also corresponds to a small value of a_0 (Figs. 2a–c), it is useful to examine the impact of the preexisting synoptic-scale eddy strength on the blocking duration, strength, and position. To compare Figs. 6 and 7, we fix the amplitude of the initial dipole planetary wave and choose a large value of a_0 but vary the strength of u_0. For $B(x, 0) = 0.4$ and $a_0 = 0.23$ we show the instantaneous planetary-scale field of the eddy-driven blocking dipole during its life cycle in Fig. 8 for $a_0 = 0.7$ and $u_0 = 0.9$. Note that when the preexisting eddy strength is stronger, the blocking dipole is more intense and rapidly westward moving, even under a strong MWW condition with large a_0 (Fig. 8b vs Fig. 6a). Because of its rapid retrogression, this blocking persistence is decreased over a given region. However, considering a strong VS condition is somewhat equivalent to choosing relatively large values of a_0 and u_0 in our barotropic NMI model. In the next section, we will consider a general case by assuming that the UB is a perturbed soliton solution. Such a study will confirm that the UB is short lived if the MWW or preexisting eddy strength is strong.

c. *The dependence of the phase speed of the blocking dipole on the blocking amplitude*

As given in appendix B, in the NMI model the phase speed of the soliton blocking in a uniform background westerly wind can be rewritten as $C_P = C_R + C_B$, where $C_R = u_0 - (\beta + Fu_0)/(k^2 + m^2 + F)$ is the phase speed of the linear Rossby wave and $C_B = -\delta M(t)^2/2k$ [$\delta > 0$ is a nonlinear term; see Luo and Li (2000) and Luo (2005) as well as appendix B] is the blocking-induced westward

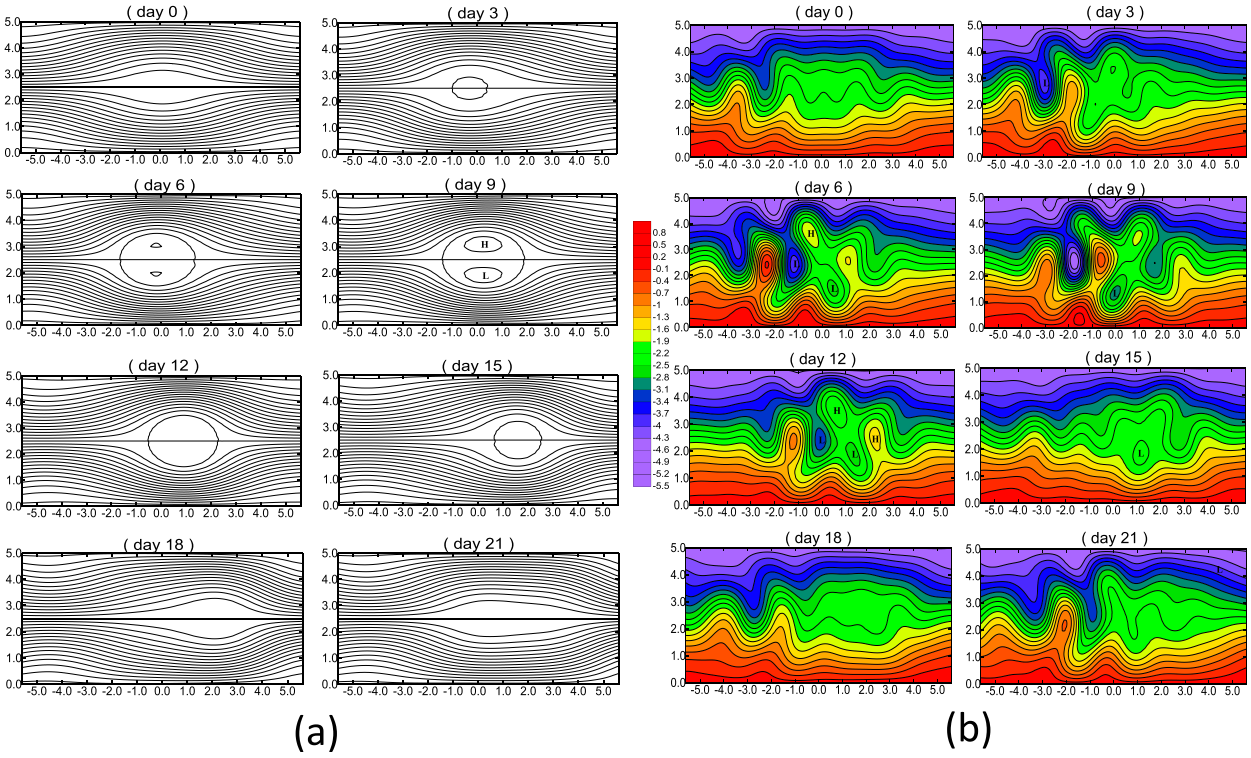

FIG. 6. (a) Planetary-scale [nondimensional; contour interval (CI) = 0.15] and (b) total streamfunction (nondimensional; CI = 0.3) fields of a blocking life cycle—from (top left) day 0 to (bottom right) day 21 in each of (a),(b)—obtained from the NMI model for a strong mean westerly wind $u_0 = 0.9$ (9 m s^{-1} in dimensional form), $a_0 = 0.17$, and the initial amplitude, $B(x, 0) = 0.4$.

speed, which depends on the blocking amplitude M. It is noted that C_R depends on the strength of the mean westerly wind. We have $C_P \approx C_R$ because $C_B \approx 0$ for $M \approx 0$. In this case, whether the small-amplitude blocking dipole shifts eastward or westward is mainly determined by the strength of the background westerly wind. When the blocking amplitude is relatively large $M \geq (2kC_R/\delta)^{1/2}$ for $C_R > 0$, its zonal displacement is controlled by a joint role of the blocking amplitude and mean westerly wind strength. In this case, the zonal movement of the blocking dipole is determined not only by the strength of the mean westerly wind but also by the blocking amplitude M. A key result is found here that when the blocking-induced westward speed exceeds the mean-flow-induced eastward speed, the blocking dipole will undergo a westward movement. This result explains why the observed large-amplitude blocking dipole has always a distinct retrogression.

It is worth pointing out that the nonlinear term δ is an important factor that measures whether a soliton block is easily established (Luo 2000, 2005). When δ is largely positive, the blocking dipole is favored. We show the value of δ against the strength of mean westerly wind u_0 in Fig. 9a and the phase speed C_P against the blocking amplitude M in Fig. 9b for $u_0 = 0.7$ and $u_0 = 0.9$. It is found that when the mean westerly wind is weaker, δ is larger and favors the appearance of a blocking dipole. That is to say, the role of Arctic warming over the BKS is to encourage the establishment of a blocking dipole over the Ural region through strengthening the nonlinearity term δ due to the reduced mean zonal wind. On the other hand, we see in Fig. 9b that the larger the blocking amplitude is, the larger the negative value of C_P is. Thus, it is inevitable that the large-amplitude blocking undergoes a marked westward displacement. In particular, when the blocking amplitude is rather large, the impact of the background westerly wind strength on the zonal movement of the blocking dipole becomes extremely weak. Thus, when the blocking amplitude is very large, the blocking-induced westward movement is dominant.

d. *Blocking position and its link with the blocking intensity*

To quantify the relationship between the blocking intensity and blocking location, it is necessary to define the blocking intensity in our NMI model. Here, the blocking intensity is defined in terms of the planetary-scale streamfunction ψ_P of the blocking dipole as given in appendix A. In the planetary-scale field, we denote the maximum (minimum) value of the northern (southern)

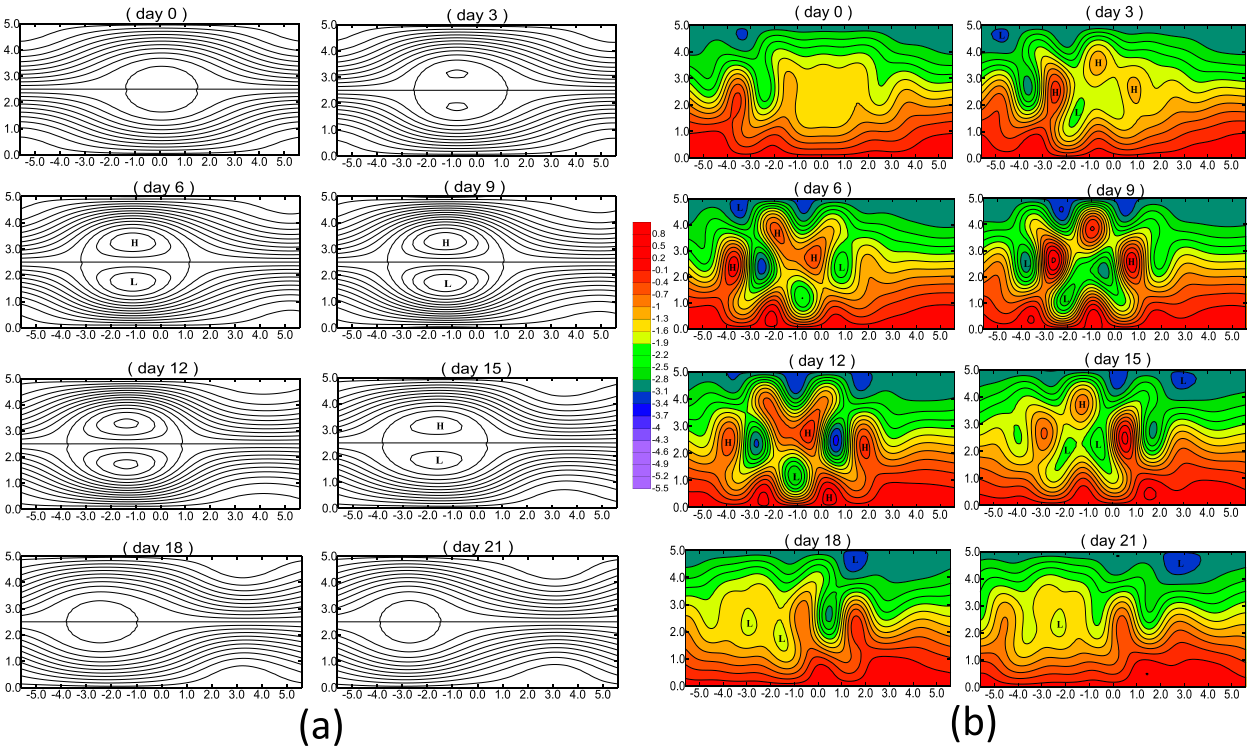

FIG. 7. As in Fig. 6, but for a weak mean westerly wind $u_0 = 0.6$ (6 m s^{-1} in dimensional form).

center of the blocking dipole as ψ_{PN} (ψ_{PS}). We then define $B_1 = |\psi_{PS} - \psi_{PN}|$ as the blocking intensity. The blocking duration is defined to be the number of consecutive days for which $B_1 \geq B_{IC}$ (where B_{IC} is the blocking threshold).

For a fixed preexisting eddy strength $a_0 = 0.17$, we show the blocking location against the blocking intensity and the time evolution of the blocking intensity in Fig. 10 for different mean westerly wind strengths and different amplitudes of the initial dipole planetary wave anomaly $B(x, 0)$. It is seen that when the initial dipole planetary wave amplitude is large (blue line in Fig. 10a) or when the mean westerly wind is weak (black line in Fig. 10a), the formed blocking dipole is intense and long lived (blue and black lines in Fig. 10b). In contrast, the blocking dipole is weak and short lived when the mean westerly wind is strong (green and red lines in Fig. 10b). This blocking dipole can become strong if a strong VS condition is considered (Luo 2000), even though the mean zonal wind is relatively strong. This is because the strong VS-induced dipole growth is larger than the strong mean zonal-wind-induced dipole suppression (not shown). In particular, we note that the large-amplitude blocking dipole (black and blue lines in Fig. 10a) is located much more westward than the small-amplitude blocking (green and red lines in Fig. 10a). Another interesting point we see in Fig. 10a is that the relationship between the blocking intensity and blocking location bears a striking resemblance to the observed result in Fig. 1c. This indicates that the NMI model can capture the main features about the quasi stationarity and persistence of UB patterns under different background conditions. The further explanation about this is presented below.

e. *Theoretical explanation of observational results*

In reality the mean zonal wind is not uniform in the zonal and meridional directions. In this case, it is convenient to decompose the mean zonal wind into two parts: a spatially uniform part u_0 and a spatially varying part $\Delta U_n(x, y)$. If one assumes that $\Delta U_n(x, y)$ is slowly varying, the "local" phase speed can be approximated as $C_P = \Delta U_n(x, y) + C_R + C_B$. It is obvious that the positive or negative value of $\Delta U_n(x, y)$ can affect the zonal movement of the blocking dipole.

As found by Luo (2000) in the case of the two-layer baroclinic NMI model, an initial dipole planetary wave can be rapidly amplified into a rather strong blocking dipole under a strong VS condition. Thus, it is not unexpected to observe a strong blocking dipole in the strong VS or MWW environment (Fig. 2a), while the strong VS often corresponds to a strong MWW as revealed in Part I. As pointed out above, the impact of the mean zonal wind strength on the zonal movement of the blocking dipole becomes unimportant when the amplitude of blocking dipole is very large. Thus, the rapid

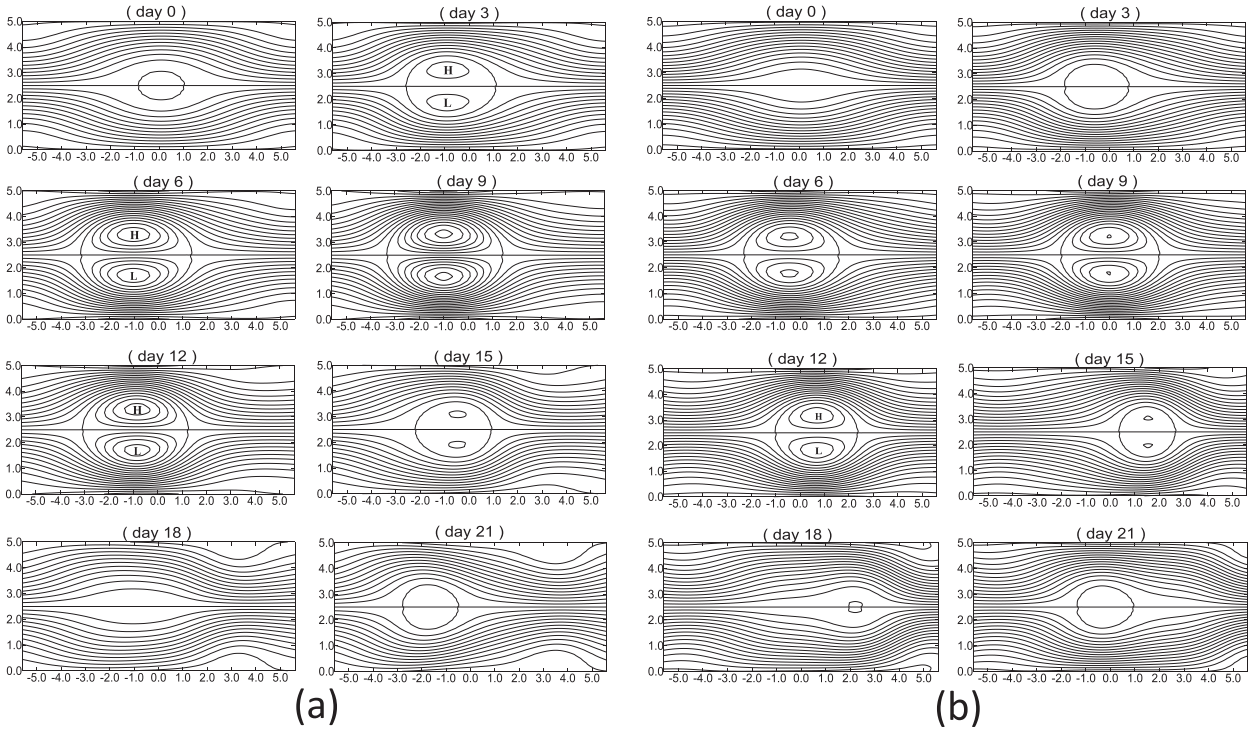

FIG. 8. Planetary-scale (nondimensional; CI = 0.15) field of a blocking life cycle obtained from the NMI model with the pre-existing eddy strength $a_0 = 0.23$ and the initial amplitude $B(x, 0) = 0.4$ for two types of background westerly wind strengths (a) $u_0 = 0.7$ and (b) $u_0 = 0.9$—from (top left) day 0 to (bottom right) day 21 in each of (a),(b).

retrogression of the strong blocking dipole is inevitably seen in Fig. 2a in that the blocking-induced westward movement is dominant. Because this large-amplitude blocking is rapidly westward traveling (Fig. 2a), it is less persistent over a given region (in our case, the Ural Mountains) even though long lived. In contrast, under a quasi-barotropic (weak MWW and VS) condition the amplification of blocking dipole is slow (Fig. 2b) so that the blocking amplitude is smaller (Fig. 1a) than that under the quasi-baroclinic (strong VS and MWW) condition. In this case, the amplitude of the UB and the strength of mean westerly wind and its spatial distribution contribute significantly to the zonal movement of the blocking dipole. The slow retrogression of blocking dipole is not only due to the blocking amplitude being smaller under the quasi-barotropic condition (red and green in Fig. 1a and Fig. 2b) but also due to the mean zonal wind being strong [$\Delta U_n(x, y)$ is positive] over the North Atlantic (Figs. 4a,b). The intensified North Atlantic westerly wind is more likely to be a response to enhanced Arctic warming over the BKS, as seen in Fig. 2f of Part I. Thus, the strong mean zonal wind over the North Atlantic tends to suppress the further retrogression of the blocking dipole from the Ural region to the European continent (Fig. 2b), while the MWW is weaker over mid–high-latitude Eurasia (Fig. 1a). This is a likely cause of why the UB pattern tends to be quasi stationary and more persistent over the Ural region under a quasi-barotropic condition.

5. The period of the UB soliton and its relationship with the background condition change

While the zonal movement and duration of the UB are found to depend on the background condition changes, it is useful to quantify how the duration of UB depends on the mean zonal wind u_0 and preexisting eddy a_0 strengths because the more persistent UB often corresponds to small values of u_0 and a_0 (Figs. 1a,c). The equation of the blocking amplitude $B(x, t)$ can be obtained and is described in appendix A.

Using the transformations $B = \tilde{B}/\sqrt{\delta}, X = (x - C_g t)/(2\lambda)^{1/2}$, and $T = t$, the forced nonlinear Schrödinger (NLS) equation in appendix A [Eq. (A2h)] can be expressed as

$$i\frac{\partial \tilde{B}}{\partial T} + \frac{1}{2}\frac{\partial^2 \tilde{B}}{\partial X^2} + |\tilde{B}|^2\tilde{B} = iP, \tag{1}$$

where

$$P = i\sqrt{\delta}Gf_0^2 \exp\{-i[\Delta k\sqrt{2\lambda}\,X + (\Delta k C_g + \Delta\omega)T]\}.$$

For uniform preexisting synoptic-scale eddies ($f_0 = a_0$ for $\mu = 0$), under the condition $\Delta k = 0$ ($\tilde{k}_2 - \tilde{k}_1 = k$ for

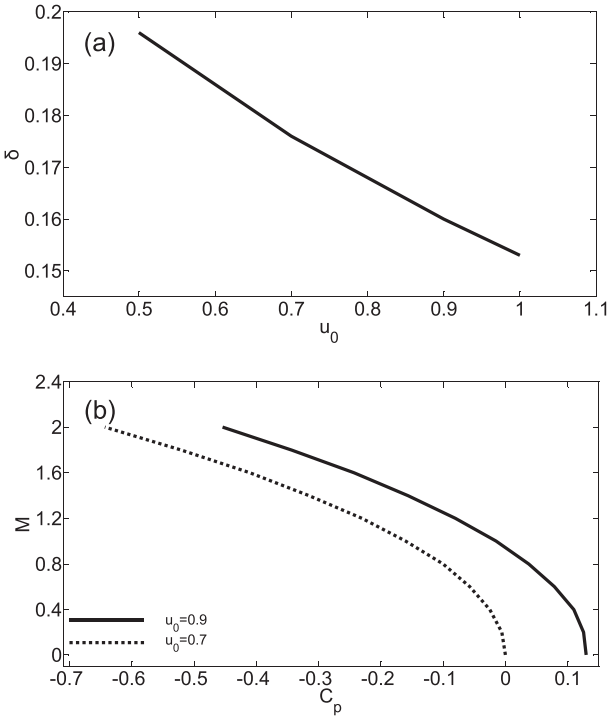

FIG. 9. (a) Nondimensional nonlinearity term δ against the nondimensional uniform westerly wind strength u_0 (the dimensional unit is $10\,\mathrm{m\,s^{-1}}$) in the NMI model and (b) the phase speed C_P (the dimensional unit is $10\,\mathrm{m\,s^{-1}}$) of the soliton block against its nondimensional amplitude M (the dimensional unit is $10^7\,\mathrm{m^2\,s^{-1}}$).

$\tilde{k}_1 = 9k_0$ and $\tilde{k}_2 = 11k_0$), the perturbed soliton solution to Eq. (1) can be assumed to be $\tilde{B} = \eta(T)\,\mathrm{sech}[\eta(T)X]\exp[i\theta(T)]$. In this case, by defining $\eta(T) = \delta^{1/2}M(t)$ and $\theta(T) = \Theta(t)$, the following nonlinear equation can be obtained:

$$\frac{dM}{dt} = Ga_0^2\sin(\Delta\omega t + \Theta) \quad \text{and} \tag{2a}$$

$$\frac{d\Theta}{dt} = \frac{\delta}{2}M^2. \tag{2b}$$

Equation (2) can describe the time variations of the blocking amplitude and phase if the soliton solution of Eq. (1) is regarded as a blocking solution. This has been demonstrated in our previous studies (Luo 2000; Luo and Li 2000). However, how the blocking duration depends on the background condition change was not examined in detail in those studies, although they have indicated that the soliton solution can capture the main features of observed blocking events. It is seen that the time variation of the blocking amplitude M depends not only on the period $2\pi/\Delta\omega$ of the preexisting eddy vorticity forcing (which is a function of the mean zonal wind u_0) but also on the preexisting eddy strength a_0. We also note that the variation of the blocking amplitude also depends on the initial amplitude itself. The long period of the blocking amplitude corresponds in general to a long-lived UB. Thus, below we will examine how the period of the blocking amplitude is dependent on the mean zonal wind and preexisting eddy strengths. For initial values $M(0) = 0.4$ and $\Theta(0) = 0$, we show the time series of the soliton amplitude M and associated phase trajectories ($M\cos\Theta$, $M\sin\Theta$) and (M, M_t) in Fig. 11 for $u_0 = 0.7$ and for four cases of $a_0 = 0.1$, 0.2, 0.3, and 0.4, where $M_t = dM/dt$. It is obvious that the soliton amplitude exhibits a periodic oscillation. This result can be seen from the phase trajectories of this soliton. For the different strength of the mean zonal wind, the duration of the soliton is shown in Fig. 12a for fixed preexisting eddy strength. The result is depicted in Fig. 12b for the different preexisting eddy strength and fixed mean zonal wind strength. We see that the soliton duration is significantly shortened as the preexisting synoptic-scale eddies are strongly intensified (Fig. 12a). Such an effect is more distinct when the mean zonal wind is weaker. The soliton duration is almost independent of the preexisting eddy strength if a_0 is smaller than 0.2. But it can depend strongly on the preexisting eddy strength if the preexisting eddies are strong enough. The decrease

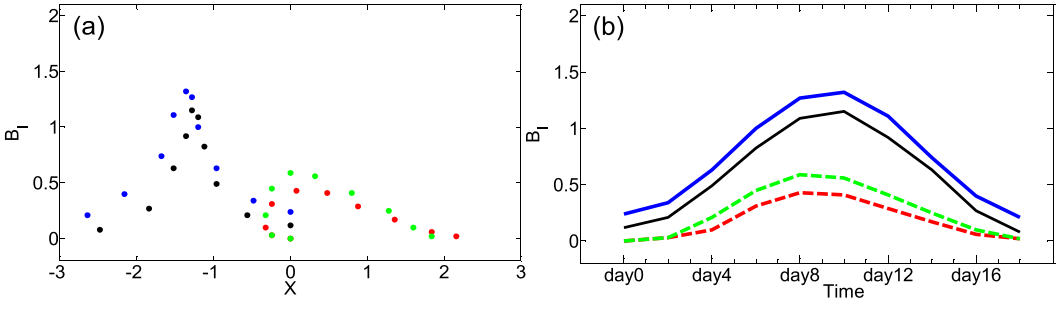

FIG. 10. (a) The blocking intensity B_1 against the zonal position of the maximum anticyclonic center of blocking and (b) its time evolution obtained from the NMI model with fixed preexisting eddy strength $a_0 = 0.17$. The black (blue) curve denotes the case of $u_0 = 0.6$ and $B(x, 0) = 0.4$ [$B(x, 0) = 0.45$], while the red (green) curve represents the case of $u_0 = 0.9$ and $B(x, 0) = 0.4$ [$B(x, 0) = 0.45$].

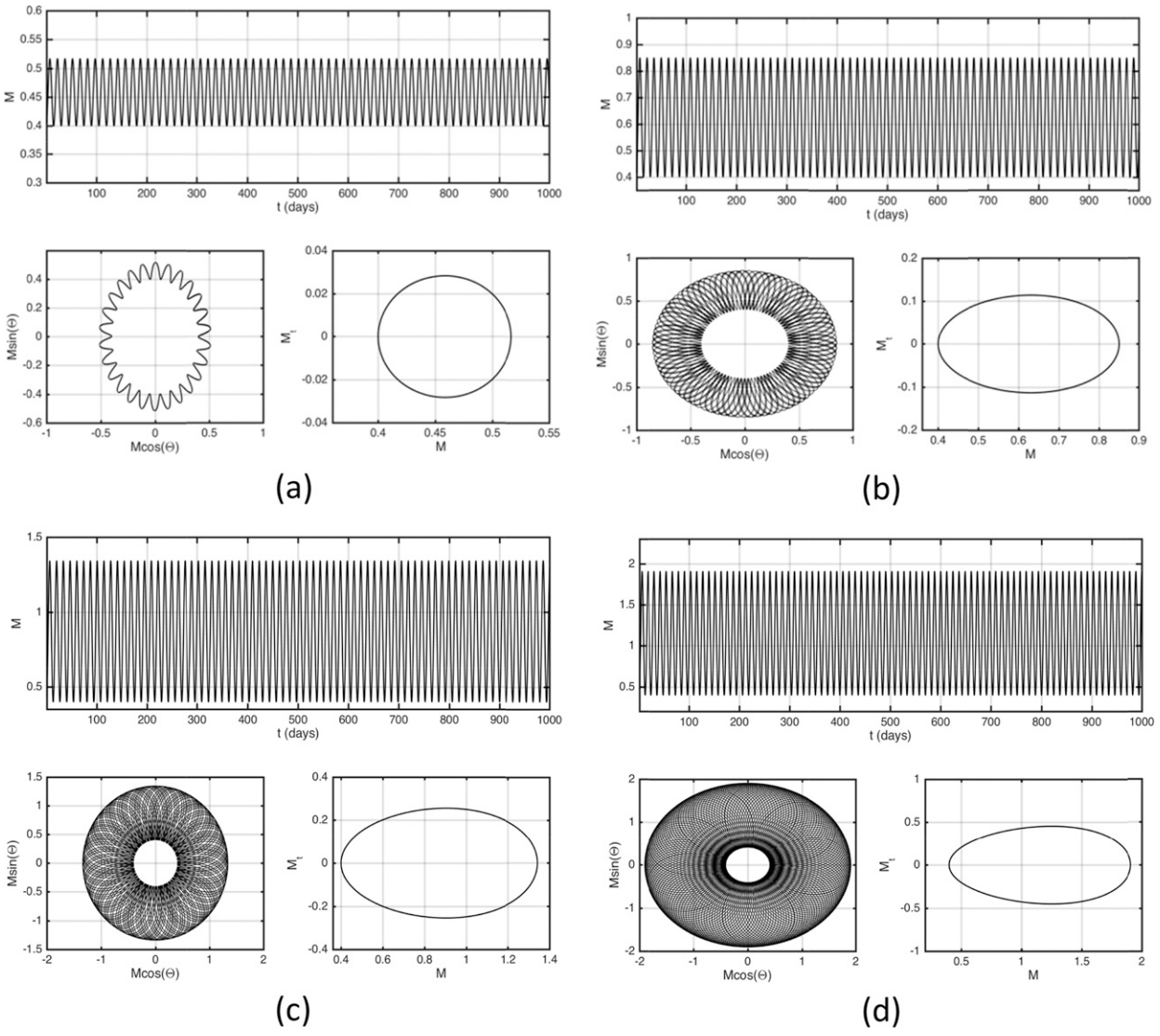

FIG. 11. Time variations of the soliton amplitude M (top panel in each of the 4 cases) and associated phase trajectories ($M\cos\Theta$ vs $M\sin\Theta$, bottom left panel in each of the 4 cases) and M vs M_t ($=dM/dt$, bottom right panel in each of the 4 cases) with $u_0 = 0.7$, and initial values $M(0) = 0.4$ and $\Theta(0) = 0$ for four cases: (a)–(d) $a_0 = 0.1$, 0.2, 0.3, and 0.4, respectively.

in the soliton duration is also dependent on the increase in the mean zonal wind. But such a decrease in the soliton duration due to the intensified mean zonal wind becomes less distinct if the preexisting synoptic-scale eddies are very strong (Fig. 12b). Thus, the blocking dipole is short lived as the mean zonal wind and preexisting eddy strengths are strong. This result is easily explained. This is because the duration of the soliton blocking depends on the amplitude itself and the period of the eddy vorticity forcing induced by preexisting synoptic-scale eddies. When the blocking amplitude is large or the period of the preexisting eddy vorticity forcing is short, the blocking duration becomes short. A larger-amplitude blocking can occur if the preexisting eddy strength is stronger, while the period of the preexisting eddy forcing becomes shorter as the mean zonal wind is stronger (Luo et al. 2007). Thus, it is natural that a short-lived soliton is inevitably seen as the MWW or preexisting eddy strength is stronger. For a general case ($k \neq 0$), a similar result can be found (not shown). Of course, the effect of the strong VS can be understood as being equivalent to the impact of the strong MWW, as noted in Part I. Similar results are found for other initial values of the soliton amplitude (not shown). Because the Arctic warming over the BKS corresponds to the weak MWW and VS over the Ural region, the strong mean zonal winds over the North Atlantic (Fig. 2f of Part I), and weak preexisting eddy strength over Europe, the

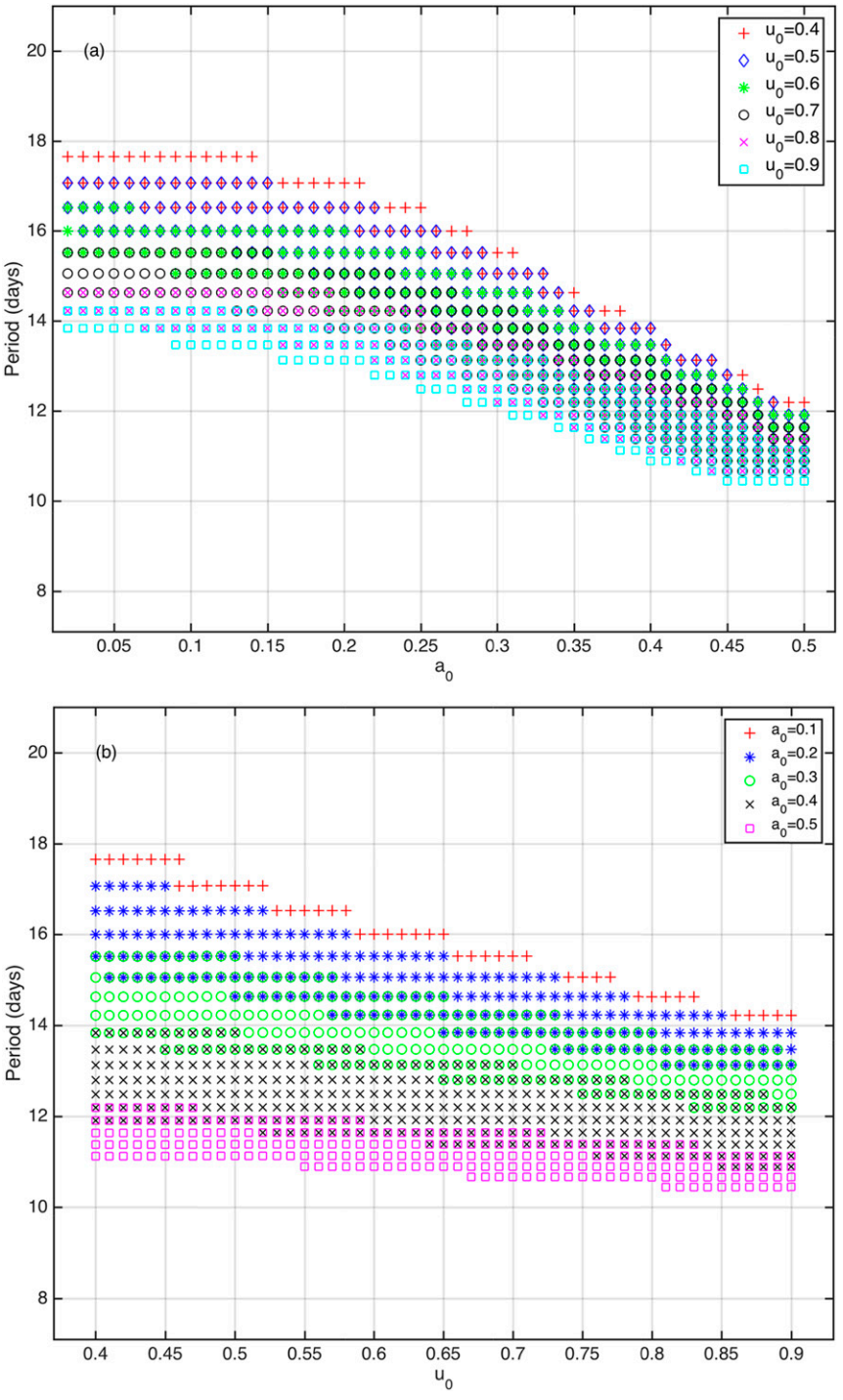

FIG. 12. The duration (days) of the perturbed soliton against the strengths of the mean zonal wind and preexisting synoptic-scale eddies: (a) the soliton duration vs the preexisting eddy strength for different mean zonal wind strengths u_0 from 0.4, 0.5, 0.6, 0.7, 0.8, and 0.9 in different colors; and (b) the soliton duration vs the mean zonal wind strength for different preexisting eddy strengths a_0 from 0.1, 0.2, 0.3, 0.4, and 0.5. (The dimensional unit is $10\,\mathrm{m\,s^{-1}}$.)

increased quasi stationarity and long persistence of UB events are inevitably seen under a quasi-barotropic condition. This provides an explanation for why the UB is more quasi stationary and persistent as a stronger BKS warming takes place.

6. Conclusions and discussion

In this paper, we have examined the cause of the increased quasi stationarity and persistence of the blocking dipole over Eurasia especially over the Ural region under quasi-barotropic (weak MWW and VS) conditions. We have found that under quasi-baroclinic (strong MWW and VS) conditions an initial dipole planetary wave can be rapidly amplified into a large-amplitude blocking dipole that undergoes a marked retrogression. The amplification of the blocking dipole is so slow that a blocking dipole with the amplitude being smaller than that under quasi-baroclinic conditions can be seen under quasi-barotropic conditions, while the winter dipole planetary wave is strong. Moreover, it is found that the mid–high-latitude mean zonal wind is stronger over the North Atlantic because of the amplified warming over the BKS but weaker over the Ural region for quasi-barotropic conditions than for quasi-baroclinic conditions. Thus, under a quasi-barotropic condition the quasi stationarity and long persistence of the blocking dipole over the Ural region is likely to be closely related to the strong mid–high-latitude mean zonal wind over the North Atlantic and the blocking amplitude being smaller for the quasi-barotropic conditions than for the quasi-baroclinic condition. Meanwhile, it is found that the persistence of the UB event is also associated with the reduced mean zonal wind over the mid–high-latitude Eurasian region and the weakened synoptic-scale eddy activity upstream of the Ural region.

A barotropic NMI model is used to provide a dynamical explanation on the increased quasi stationarity and persistence of the blocking dipole over the Ural region under the quasi-barotropic condition. We find that the formed blocking dipole is of large amplitude, long lived, and westward traveling if the mean westerly wind is weak in the blocking region. It becomes quasi stationary once a strong mid–high-latitude mean zonal wind appears in the upstream of the blocking region. In particular, a strong blocking dipole can also be formed in a strong background westerly wind if the preexisting eddy strength is strong enough (Luo 2000). Moreover, based on this NMI model, the phase speed formula of the soliton block is obtained, which is different from the linear Rossby wave theory. In the linear Rossby wave theory, the phase speed of the blocking dipole is independent of the blocking amplitude, and its phase speed is only dependent on the strength of mean westerly wind and its wavelength. Obviously, this linear theory cannot explain why the large-amplitude blocking shifts rapidly westward, as seen for the quasi-baroclinic conditions (Fig. 2a). However, in the nonlinear case the phase speed of the soliton blocking is dependent not only on the strength of mean westerly wind but also on the blocking amplitude. When the blocking amplitude is so large that the blocking-induced westward speed exceeds the mean-flow-induced eastward speed, the retrograde movement of the blocking dipole occurs. In particular, when the blocking amplitude is particularly large, the mean-flow-induced eastward movement becomes unimportant so that the blocking-induced westward displacement is dominant. Of course, the persistence of the UB can be estimated in terms of the UB duration even though the long duration of the UB does not correspond to its long persistence. But the long persistence of the UB has to be long lived. The long duration of the UB means that the UB has a large incidence that allows the UB to be more persistent. Our soliton solution further reveals that the duration of the UB is longer as the mean zonal wind over the Ural region or the strength of preexisting synoptic-scale eddies upstream of the Ural region is weaker (Fig. 12). Thus, the quasi stationarity and persistence of the UB is related not only to the reduced (enhanced) mean zonal wind and its weak (strong) vertical shear over the Ural region (North Atlantic) but also to the reduced synoptic-scale eddy activity upstream of the Ural region. The changes in the parameters are closely associated with the Arctic warming over the BKS.

On the other hand, because the blocking dipole is particularly strong under the quasi-baroclinic condition, the blocking-induced westward shift is dominant so that a marked retrogression of the blocking dipole can be seen in Fig. 2a. But under the quasi-barotropic condition the amplitude of the UB is relatively small compared to the quasi-baroclinic case. In this case, it can undergo a distinct westward shift if the zonal wind is uniform and weak, even though its amplitude is small. However, because the mean westerly wind is strong over the North Atlantic west of 0° longitude in Fig. 4a (west of 15°E in Fig. 4b) owing to the Arctic warming over the BKS, it suppresses the further retrogression of the blocking dipole from the Ural region to the European continent. In this case, the blocking dipole becomes easily quasi stationary. Such a westerly wind distribution is closely related to the warming over the BKS, as revealed in Part I. Hence, the blocking dipole tends to be quasi stationary and persistent over the Ural region under a quasi-barotropic condition related to the Arctic warming over the BKS. In summary, how the BKS warming affects the duration and

movement of the UB can be described in Fig. 13 as a schematic diagram. This figure shows that the role of the BKS warming is to suppress the retrogression of the UB and to lengthen its duration through the strengthening (weakening) of mid–high-latitude westerly winds over the North Atlantic (Eurasia, mainly in the Ural region and its downstream side), then leading to a more quasi-stationary and persistent UB.

However, it must be pointed out that although the NMI model can explain the main features of the blocking dipole, a full explanation will require the extension of the model to include baroclinic effects and background conditions. This challenge will be addressed in future work.

Acknowledgments. The first two authors acknowledge the support from the National Natural Science Foundation of China (Grants 41430533, 41375067, and 41505075) and the National Key Research and Development Program of China (2016YFA0601802). A. Dai is supported by the U.S. National Science Foundation (Grant AGS-1353740), U.S. Department of Energy's Office of Science (Award DE-SC0012602), and the U.S. National Oceanic and Atmospheric Administration (Award NA15OAR4310086). I. Simmonds was supported by Australian Research Council Grant DP 160101997. The authors thank three anonymous reviewers for their very valuable suggestions on the original submission.

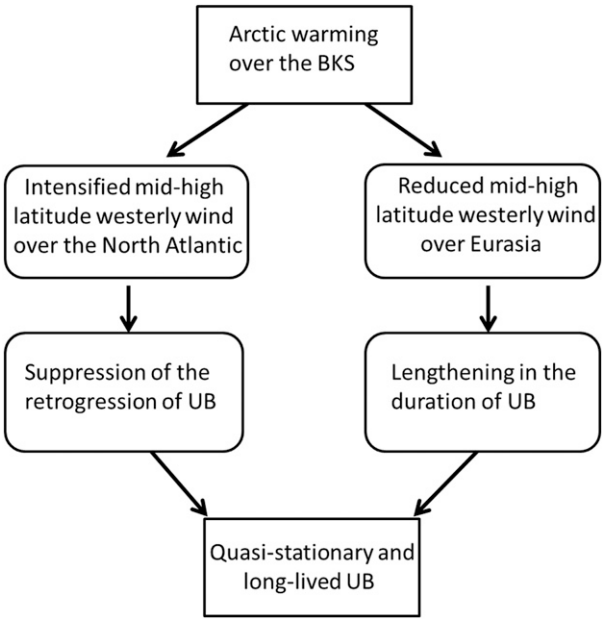

FIG. 13. Schematic diagram of the Arctic warming in the BKS affecting the duration and movement of the UB through the weakening (strengthening) of mid–high-latitude westerly winds over Eurasia (the North Atlantic).

APPENDIX A

Nonlinear Multiscale Interaction Model of Blocking Events and Its Solution

Here, we describe the nonlinear multiscale interaction (NMI) model developed by Luo (2000, 2005), Luo and Li (2000), and Luo et al. (2001, 2014). This model is very efficient for representing the life cycle of observed meandering blocking flows, which was also extended to examine the North Atlantic Oscillation (NAO) dynamics (Luo et al. 2007). To reduce the complexity of our problem, we make the assumption that an equivalent barotropic model is an appropriate choice to describe the movement and structure of the UB. Because the negative phase of NAO resembles a blocking flow over North Atlantic, the NAO model of Luo et al. (2007) is applicable to the explanation of a blocking process. Moreover, because our focus is on the zonal movement and period of the UB, the effect of the VS on the movement and period of UB can be explored by assuming that the UB has larger amplitude in a quasi-barotropic condition to illustrate an analogy with a quasi-baroclinic case. Such an assumption can allow us to unify the two cases into a barotropic model.

Here, let us define a planetary-scale component as zonal wavenumber k and a synoptic-scale eddy component as zonal wavenumber $\tilde{k}_j$. Under the zonal-scale separation assumption $k \ll \tilde{k}_j$, it is easy to obtain the following nondimensional barotropic potential vorticity (PV) equations of the nonlinear planetary-to-synoptic-scale interaction in a uniform westerly wind u_0 and in a beta-plane channel with the width of L_y (Luo 2000, 2005; Luo and Li 2000; Luo et al. 2001; 2014):

$$\left(\frac{\partial}{\partial t}+u_0\frac{\partial}{\partial x}\right)(\nabla^2\psi - F\psi) + J(\psi,\nabla^2\psi) + (\beta + Fu_0)\frac{\partial\psi}{\partial x} = -\nabla\cdot(\mathbf{v}'q')_P \quad \text{and} \tag{A1a}$$

$$\left(\frac{\partial}{\partial t}+u_0\frac{\partial}{\partial x}\right)(\nabla^2\psi' - F\psi') + (\beta + Fu_0)\frac{\partial\psi'}{\partial x} = -J(\psi',\nabla^2\psi) - J(\psi,\nabla^2\psi') + \nabla^2\psi_S^*, \tag{A1b}$$

where $\nabla\cdot(\mathbf{v}'q')_P = J(\psi' q')_P$ is a planetary-scale component that has a zonal wavenumber close to that of the projection of the planetary-scale blocking flow (Luo 2000, 2005; Luo and Li 2000; Luo et al. 2001) or the NAO pattern (Luo et al. 2007), $\mathbf{v}' = (-\partial\psi'/\partial y, \partial\psi'/\partial x)$, $q' = \nabla^2\psi'$, $F = (L/R_d)^2$, and ψ and ψ' are planetary- and synoptic-scale anomalies, respectively. Here, R_d is the

radius of Rossby deformation that satisfies $F = 1$, $\beta = [(2 \times 7.29)/6.371]\cos(\phi_0)$ is the nondimensional meridional gradient of the Coriolis parameter at a given reference latitude ϕ_0, and $\nabla^2\psi_S^*$ is the synoptic-scale wavemaker designed to maintain the preexisting synoptic-scale eddies prior to the block onset. Also note that in Eq. (A1) all the variables have been nondimensionalized by characteristic length $L = 10^6$ m and velocity $U = 10\,\mathrm{m\,s^{-1}}$. If we set $L_y = 5$, then it represents the meridional width of 5000 km. The two-scale interaction equations of planetary- and synoptic-scale motions in baroclinic and barotropic flows were first obtained by Luo (2000), Luo and Li (2000), and Luo et al. (2001) and then further simplified into Eq. (A1) by Luo (2005) under some assumptions. When $\nabla^2\psi_S^*$ vanishes and when $J(\psi', q')_S$ is included [where $J(\psi', q')_S$ denotes synoptic-scale component of $J(\psi', q')$], Eq. (A1) reduces to the planetary-to-synoptic interaction equation derived by Luo and Li (2000), which was also extended to include the horizontal shear of the basic flow (Luo et al. 2001). This NMI model is clearly different from the low-to-high-frequency interaction equation presented by Haines and Holland (1998), which cannot be analytically solved. Our model is also different from the previous eddy–mean flow interaction models (Hoskins et al. 1983) because the time-mean eddy forcing $\nabla \cdot \overline{(\mathbf{v}'q')}$ is only included in those models. In this NMI model, the blocking evolution and its associated mean flow variation can be described by Eq. (A1a) because $\nabla \cdot (\mathbf{v}'q')_P$ in this equation is time varying. Moreover, because Eq. (A1b) includes the feedback of the time-varying blocking flow ψ, the synoptic eddies will exhibit the same low-frequency variation as that of the blocking flow during their interaction process. Obviously, the previous models cannot describe such low-frequency variations of the blocking pattern and synoptic-scale eddies during their interaction because a time average is often used to derive the large-scale PV equation.

Different from previous blocking theories (McWilliams 1980; Shutts 1983), the NMI model (Luo 2000, 2005; Luo et al. 2001, 2014) can describe the life cycles of observed blocking flows (Berggren et al. 1949; Holopainen and Fortelius 1987). Thus, it is feasible to use the NMI model to examine how the blocking duration, strength, and position depend on changes in the background parameters in response to Arctic warming associated with the BKS sea ice loss.

The basic idea of the NMI model is that the development of a meandering blocking flow is determined by the spatial structure of preexisting synoptic-scale eddies (Luo 2000, 2005; Luo and Li 2000; Luo et al. 2014) rather than by the eddy straining or wave breaking (Shutts 1983). The merit of this theory is that it is able to give us some useful information about how the duration, strength, and position of a blocking event depend on changes in atmospheric background parameters.

It is also useful to rewrite Eq. (A1a) as

$$\frac{\partial q}{\partial t} + J(\psi - u_0 y, \nabla^2\psi + \beta y) = -\nabla \cdot (\mathbf{v}'q')_P,$$

where $q = \nabla^2\psi - F\psi$. In general, a blocking flow satisfies $J(\psi - u_0 y, \nabla^2\psi + \beta y) \approx 0$. In this case, one can obtain

$$\frac{\partial q}{\partial t} \approx -\nabla \cdot (\mathbf{v}'q')_P.$$

Thus, whether the blocking anomaly can grow or decay depends on the sign and spatial structure of $-\nabla \cdot (\mathbf{v}'q')_P$. The blocking can be formed only when $-\nabla \cdot (\mathbf{v}'q')_P$ matches its PV field. This is the so-called eddy-blocking matching mechanism proposed by Luo et al. (2014). According to the work of Luo (2000, 2005), synoptic-scale eddies can be decomposed into two parts: preexisting synoptic-scale eddies ψ_1' and deformed eddies ψ_2' induced by the intensified blocking in the form of $\psi' = \psi_1' + \psi_2'$. During the initial stage ($t \sim 0$) of a blocking flow, the growth of the blocking is determined by the spatial structure of $-\nabla \cdot (\mathbf{v}_1'q_1')_P$ because $\partial q/\partial t \approx -\nabla \cdot (\mathbf{v}_1'q_1')_P$ as a result of $\psi_2' \approx 0$ for an initial blocking flow being weak. This indicates that the blocking formation is dominated by preexisting synoptic-scale eddies, rather than by deformed eddies. In other words, the eddy straining or wave breaking is unimportant for the blocking establishment. Thus, the eddy straining mechanism of Shutts (1983) may be inappropriate for the generation of blocking and its life cycle. In our NMI model, the spatial structure of preexisting synoptic-scale eddies is crucial for the blocking generation (Luo 2000, Luo and Li 2000; Luo et al. 2001, 2014). Based on the above considerations, the analytical solution of Eq. (A1) can be derived for an eddy-driven blocking flow by using an asymptotic expansion method as used in Luo (2000, 2005) and Luo et al. (2007, 2014).

According to Luo et al. (2007), the analytical solution of Eq. (A1) can be expressed as follows:

$$\Psi_T = -u_0 y + \psi + \psi' = \psi_P + \psi', \tag{A2a}$$

$$\psi_P = -u_0 y + \psi \approx -u_0 y + \psi_B + \psi_m, \tag{A2b}$$

$$\psi_B = B\sqrt{\frac{2}{L_y}}\exp[i(kx - \omega t)]\sin(my) + \mathrm{cc}, \tag{A2c}$$

$$\psi_m = -|B|^2 \sum_{n=1}^{\infty} q_n g_n \cos(n + 1/2)\, my, \tag{A2d}$$

$$\psi' \approx \varepsilon^{3/2}(\tilde{\psi}_0' + \varepsilon\tilde{\psi}_1') = \psi_1' + \psi_2', \tag{A2e}$$

$$\psi_1' = \varepsilon^{3/2}\tilde{\psi}_0' = f_0(x)\{\alpha_1 \exp[i(\tilde{k}_1 x - \tilde{\omega}_1 t)] + \alpha_2 \exp[i(\tilde{k}_2 x - \tilde{\omega}_2 t)]\}\sin\left(\frac{m}{2}y\right) + \mathrm{cc}, \tag{A2f}$$

$$\psi_2' = -\frac{m}{4}\sqrt{\frac{2}{L_y}}Bf_0\sum_{j=1}^{2}Q_j\alpha_j\exp\{i[(\tilde{k}_j+k)x-(\tilde{\omega}_j+\omega)t]\}\left[p_j\sin\left(\frac{3m}{2}y\right)+r_j\sin\left(\frac{m}{2}y\right)\right]$$
$$+\frac{m}{4}\sqrt{\frac{2}{L_y}}B^*f_0\sum_{j=1}^{2}Q_j\alpha_j\exp\{i[(\tilde{k}_j-k)x-(\tilde{\omega}_j-\omega)t]\}\left[s_j\sin\left(\frac{3m}{2}y\right)+h_j\sin\left(\frac{3m}{2}y\right)\right]+\text{cc}, \quad \text{and} \qquad \text{(A2g)}$$

$$i\left(\frac{\partial B}{\partial t}+C_g\frac{\partial B}{\partial x}\right)+\lambda\frac{\partial^2 B}{\partial x^2}+\delta|B|^2B$$
$$+Gf_0^2\exp[-i(\Delta kx+\Delta\omega t)]=0, \qquad \text{(A2h)}$$

where $\Delta k = k-(\tilde{k}_2-\tilde{k}_1)$, $\Delta\omega=\tilde{\omega}_2-\tilde{\omega}_1-\omega$, $\tilde{\omega}_j = u_0\tilde{k}_j-(\beta+Fu_0)\tilde{k}_j/(\tilde{k}_j^2+m^2/4+F)$ $(j=1, 2)$, $\omega = u_0k-(\beta+Fu_0)k/(k^2+m^2+F)$, $\alpha_1=1$, $\alpha_2=\alpha$, $C_g=u_0-(\beta+Fu_0)(m^2+F-k^2)/(k^2+m^2+F)^2$, $\lambda=[3(m^2+F)-k^2](\beta+Fu_0)k/(k^2+m^2+F)^3$, $\delta=km\sum_{n=1}^{\infty}q_ng_n^2[k^2+m^2-m^2(n+1/2)^2]/(k^2+m^2+F)$, $q_n=4k^2m/L_y\{\beta+Fu_0-(u_0-C_g)[F+m^2(n+1/2)^2]\}$, $g_n=8/m[4-(n+1/2)^2]L_y$, and other coefficients can be found in Luo and Li (2000), Luo (2005), and Luo et al. (2007). Here, we assume $f_0(x)=a_0e^{-\varepsilon^2\mu(x+x_0)^2}$ to represent the amplitude of preexisting eddies having two close zonal wavenumbers $\tilde{k}_1$ and $\tilde{k}_2$ with the corresponding frequencies $\tilde{\omega}_1$ and $\tilde{\omega}_2$ that satisfy $\tilde{k}_2-\tilde{k}_1\approx k$. Moreover, ψ_B is the blocking dipole anomaly with zonal and meridional wavenumbers k and m. As in Luo (2000, 2005) and Luo et al. (2007), we may fix the parameters $\mu=1.2$, $\varepsilon=0.24$, and $x_0=2.87/2$ to make preexisting eddies locate in the upstream side of the initial blocking flow but allow the preexisting eddy strength a_0 to be a variable. In the model given in Eq. (A2), $\alpha=-1$ and $m=-2\pi/L$ represent a blocking flow or a negative NAO phase with the complex amplitude $B(x, t)$, and B^* is the complex conjugate of $B(x, t)$. Equation (A2h) is a nonlinear Schrödinger equation with an eddy forcing term that describes the space–time evolution of a blocking dipole. It should be pointed out that Ψ_T is the total field of the blocking flow, while ψ_P (ψ') is the planetary- (synoptic-) scale field of the blocking flow. The detail description of the model equation can be found in Luo et al. (2007, 2014).

It is clear that in this NMI model both the blocking anomaly and synoptic-scale eddies possess the same low-frequency time scale because the solution of deformed eddies contains the blocking amplitude. The most key parameters of the NMI model are the preexisting eddy strength a_0, mean zonal wind u_0, and amplitude $B(x, 0)$ of the initial blocking. The solution to Eq. (A2h) can be obtained by a numerical solution (Luo 2005) if the three parameters are given. Except for the three parameters, the other parameters are chosen to be the same as in Luo et al. (2014).

APPENDIX B

Phase Speed of the Soliton Block

The soliton can preserve its shape if the eddy forcing is a small perturbation to a soliton solution of Eq. (A2h) (Hasegawa and Kodama 1995). In other words, the eddy forcing does not distort the soliton shape, while the amplitude and phase of this soliton can be changed with time. In this case, we can approximate the soliton solution of Eq. (A2h) as a solution of an unforced equation. While the phase speed of the soliton is the same for forced and unforced equations, the soliton amplitude is a time function for a forced case. Naturally, the phase speed of the soliton blocking obtained by Luo [2000, C_A in his Eq. (36)] is time dependent and applicable to the explanation of the blocking movement. Correspondingly, the phase speed of the time-dependent soliton blocking can be approximately expressed as (Luo 2000)

$$C_P = u_0-\frac{\beta+Fu_0}{k^2+m^2+F}-\frac{\delta M(t)^2}{2k}, \qquad \text{(B1)}$$

where C_P is the phase velocity of the blocking dipole, and $M(t)=\max|B(x, t)|$ denotes the maximum amplitude of the blocking dipole anomaly at every day. The calculation shows that for zonal wavenumbers ~(1–3), there are $\lambda>0$ and $\delta>0$ for a dipole mode. Thus, the blocking amplitude can cause a westward shift of the blocking dipole itself because of $\delta>0$. Equation (B1) can also be derived from the combination of Eq. (A2c) and Eq. (2b).

It is seen that the phase speed of the soliton block depends on the wavenumber (k, m) and amplitude $M(t)$ of the blocking as well as the strength of the background westerly wind u_0.

Thus, for a given wavenumber, the phase speed from Eq. (B1) of the soliton blocking can be used to explain the zonal movement of the blocking dipole under different background conditions and different blocking amplitude.

REFERENCES

Berggren, R., B. Bolin, and C.-G. Rossby, 1949: An aerological study of zonal motion, its perturbations and break-down. *Tellus*, **1A**, 14–37, doi:10.1111/j.2153-3490.1949.tb01257.x.

Charney, J. G., and J. G. DeVore, 1979: Multiple flow equilibria in the atmosphere and blocking. *J. Atmos. Sci.*, **36**, 1205–1216, doi:10.1175/1520-0469(1979)036<1205:MFEITA>2.0.CO;2.

Colucci, S. J., 1985: Explosive cyclogenesis and large-scale circulation changes: Implications of atmospheric blocking. *J. Atmos. Sci.*, **42**, 2701–2717, doi:10.1175/1520-0469(1985)042<2701:ECALSC>2.0.CO;2.

Francis, J. A., and S. J. Vavrus, 2015: Evidence for a wavier jet stream in response to rapid Arctic warming. *Environ. Res. Lett.*, **10**, 014005, doi:10.1088/1748-9326/10/1/014005.

Haines, K., and A. J. Holland, 1998: Vacillation cycles and blocking in a channel. *Quart. J. Roy. Meteor. Soc.*, **124**, 873–895, doi:10.1002/qj.49712454711.

Hasegawa, A., and Y. Kodama, 1995: *Solitons in Optical Communications*. Clarendon Press, 320 pp.

Holopainen, E. O., and C. Fortelius, 1987: High-frequency transient eddies and blocking. *J. Atmos. Sci.*, **44**, 1632–1645, doi:10.1175/1520-0469(1987)044<1632:HFTEAB>2.0.CO;2.

Hoskins, J. B., I. N. James, and G. H. White, 1983: The shape, propagation and mean-flow interaction of large-scale weather systems. *J. Atmos. Sci.*, **40**, 1595–1612, doi:10.1175/1520-0469(1983)040<1595:TSPAMF>2.0.CO;2.

Inoue, J., M. E. Hori, and K. Takaya, 2012: The role of Barents Sea ice in the wintertime cyclone track and emergence of a warm-Arctic cold-Siberian anomaly. *J. Climate*, **25**, 2561–2568, doi:10.1175/JCLI-D-11-00449.1.

Kalnay, E., and Coauthors, 1996: The NCEP/NCAR 40-Year Reanalysis Project. *Bull. Amer. Meteor. Soc.*, **77**, 437–471, doi:10.1175/1520-0477(1996)077<0437:TNYRP>2.0.CO;2.

Luo, D., 2000: Planetary-scale baroclinic envelope Rossby solitons in a two-layer model and their interaction with synoptic-scale eddies. *Dyn. Atmos. Oceans*, **32**, 27–74, doi:10.1016/S0377-0265(99)00018-4.

——, 2005: A barotropic envelope Rossby soliton model for block–eddy interaction. Part I: Effect of topography. *J. Atmos. Sci.*, **62**, 5–21, doi:10.1175/1186.1.

——, and J. Li, 2000: Barotropic interaction between planetary- and synoptic-scale waves during the life cycle of blockings. *Adv. Atmos. Sci.*, **17**, 649–670, doi:10.1007/s00376-000-0026-5.

——, F. Huang, and Y. Diao, 2001: Interaction between antecedent planetary-scale envelope soliton blocking anticyclone and synoptic-scale eddies: Observations and theory. *J. Geophys. Res.*, **106**, 31 795–31 816, doi:10.1029/2000JD000086.

——, A. Lupo, and H. Wan, 2007: Dynamics of eddy-driven low frequency dipole modes. Part I: A simple model of North Atlantic Oscillations. *J. Atmos. Sci.*, **64**, 3–28, doi:10.1175/JAS3818.1.

——, J. Cha, L. Zhong, and A. Dai, 2014: A nonlinear multiscale interaction model for atmospheric blocking: The eddy-blocking matching mechanism. *Quart. J. Roy. Meteor. Soc.*, **140**, 1785–1808, doi:10.1002/qj.2337.

——, Y. Xiao, Y. Yao, A. Dai, I. Simmonds, and C. L. E. Franzke, 2016a: Impact of Ural blocking on winter warm Arctic–cold Eurasian anomalies. Part I: Blocking-induced amplification. *J. Climate*, **29**, 3925–3947, doi:10.1175/JCLI-D-15-0611.1.

——, ——, Y. Diao, A. Dai, C. L. E. Franzke, and I. Simmonds, 2016b: Impact of Ural blocking on winter warm Arctic–cold Eurasian anomalies. Part II: The link to the North Atlantic Oscillation. *J. Climate*, **29**, 3949–3971, doi:10.1175/JCLI-D-15-0612.1.

McWilliams, J. C., 1980: An application of equivalent modons to atmospheric blocking. *Dyn. Atmos. Oceans*, **5**, 43–66, doi:10.1016/0377-0265(80)90010-X.

Mu, M., and Z. Jiang, 2008: A method to find perturbations that trigger blocking onset: Conditional nonlinear optimal perturbations. *J. Atmos. Sci.*, **65**, 3935–3946, doi:10.1175/2008JAS2621.1.

Murray, R. J., and I. Simmonds, 1995: Responses of climate and cyclones to reductions in Arctic winter sea ice. *J. Geophys. Res.*, **100**, 4791–4806, doi:10.1029/94JC02206.

Overland, J., J. Francis, R. Hall, E. Hanna, S. Kim, and T. Vihma, 2015: The melting Arctic and midlatitude weather patterns: Are they connected? *J. Climate*, **28**, 7917–7932, doi:10.1175/JCLI-D-14-00822.1.

Screen, J. A., and I. Simmonds, 2013a: Exploring links between Arctic amplification and mid-latitude weather. *Geophys. Res. Lett.*, **40**, 959–964, doi:10.1002/grl.50174.

——, and ——, 2013b: Caution needed when linking weather extremes to amplified planetary waves. *Proc. Natl. Acad. Sci. USA*, **110**, E2327, doi:10.1073/pnas.1304867110.

——, C. Deser, I. Simmonds, and R. Tomas, 2014: Atmospheric impacts of Arctic sea-ice loss, 1979–2009: Separating forced change from atmospheric internal variability. *Climate Dyn.*, **43**, 333–344, doi:10.1007/s00382-013-1830-9.

Shutts, G. J., 1983: The propagation of eddies in diffluent jetstreams: Eddy vorticity forcing of 'blocking' flow fields. *Quart. J. Roy. Meteor. Soc.*, **109**, 737–761, doi:10.1002/qj.49710946204.

Simmonds, I., 2015: Comparing and contrasting the behaviour of Arctic and Antarctic sea ice over the 35-year period 1979–2013. *Ann. Glaciol.*, **56**, 18–28, doi:10.3189/2015AoG69A909.

Walsh, J. E., 2014: Intensified warming of the Arctic: Causes and impacts on middle latitudes. *Global Planet. Change*, **117**, 52–63, doi:10.1016/j.gloplacha.2014.03.003.

Yao, Y., D. Luo, A. Dai, and I. Simmonds, 2017: Increased quasi stationarity and persistence of Ural blocking and Eurasian extreme cold events in response to Arctic warming. Part I: Insights from observational analyses. *J. Climate*, **30**, 3549–3568, doi:10.1175/JCLI-D-16-0261.1.